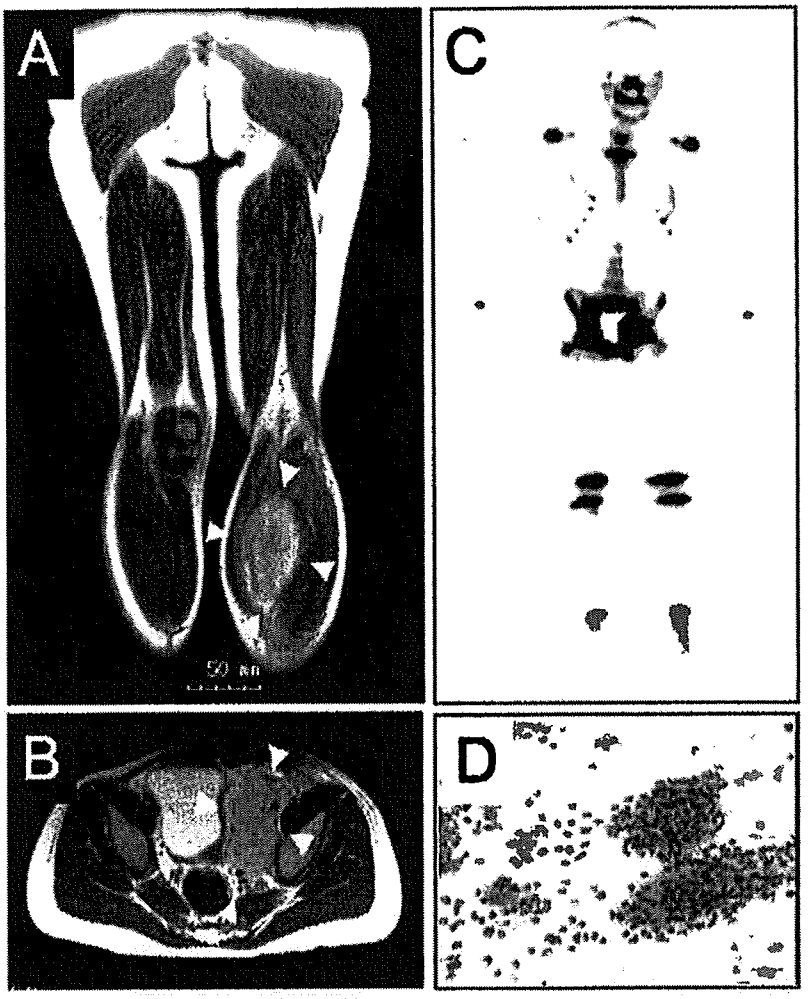

FIGURE 1 Studies at diagnosis. T2-weighted MRI images showing a mass on left leg (A, arrowheads) and metastatic swelling of para-aortic lymph nodes (B, arrowheads). (C) Scintigraphy of bone showed uptakes on right parietal, right 4th rib, and thoracic vertebrae. (D) Bone marrow aspiration showed aggregation of tumor cells.

She had HLA-A*2402 and her cancer tissue was determined by immunohistochemistry to express WT1 protein (Figure 3). She met the criteria for entry into the WT1 peptide-based clinical trial. Intradermal injection of the modified 9-mer WT1 peptide (1 mg) emulsified with Montanide ISA51 adjuvant was started from April 2005, 3 months after the last therapy (radiotherapy on the metastatic site) and continued at 1-week intervals.

The newlesions on the lumbar vertebrae remained weakly positive at the start of WT1 peptide vaccination (Figure 2B), but became negative after 3 months (12 courses) of weekly injections (Figure 2C). At 14 and 21 months after starting vaccination, scintigraphic uptake remained negative (Figure 2D, E).

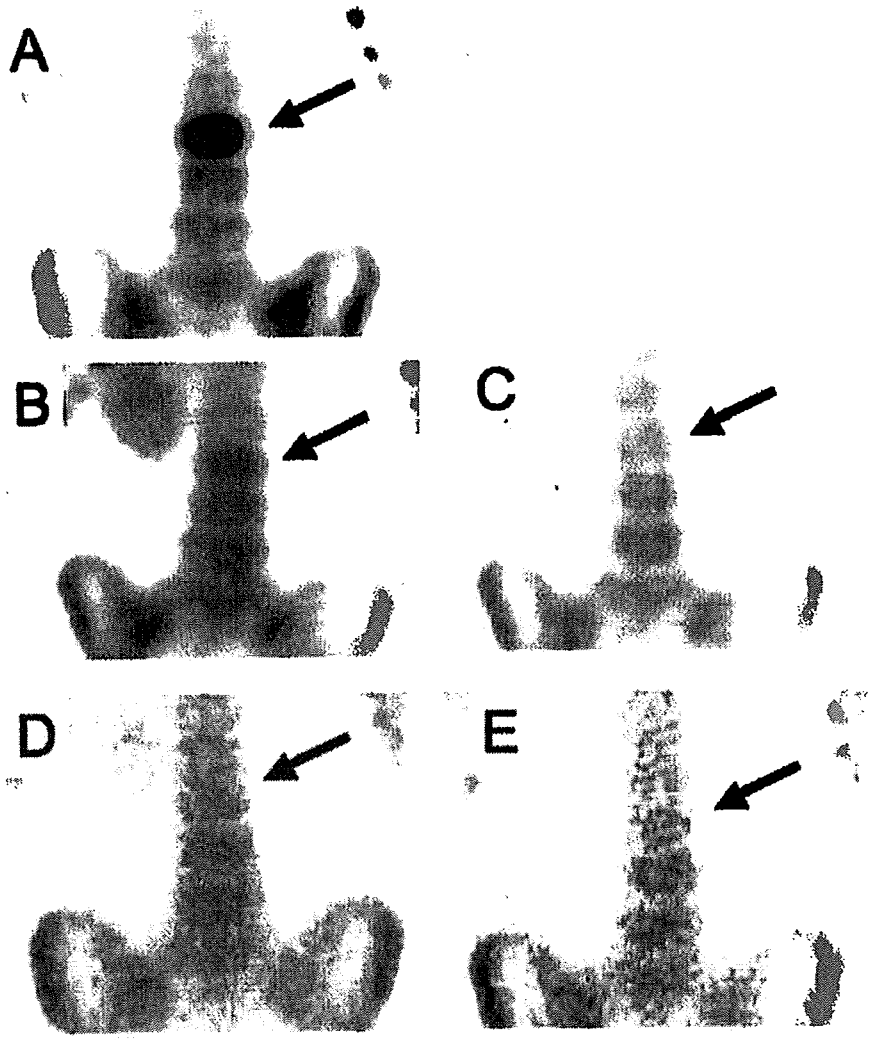

FIGURE 2 Control of new lesions of bone metastasis after the start of WT1 immunotherapy. (A) New lesions (L2, 3, 4) were observed on bone scintigraphy after two courses of combination chemotherapy. Bone scintigraphy before (B) and 3 (C), 14 (D), and 21 (E) months after WT1 vaccination. Scintigraphic uptake disappeared after vaccination. Arrow indicates L2 vertebra.

To evaluate immunological responses to WT1 peptide vaccination, WT1-specific CTL frequencies in peripheral blood and their differentiation state were analyzed by flow cytometry using WT1 tetramer. The frequency of tetramer$^+$CD8$^+$ T cells among CD8$^+$ T cells was defined as the WT1-specific CTL frequency. The frequency increased from 0.24% before vaccination to 0.37% at 1 month after the start of vaccination (1.54-fold increase). The frequency decreased to the prevaccination level at 4 months, and this was maintained at 13 months. It has recently been shown that these

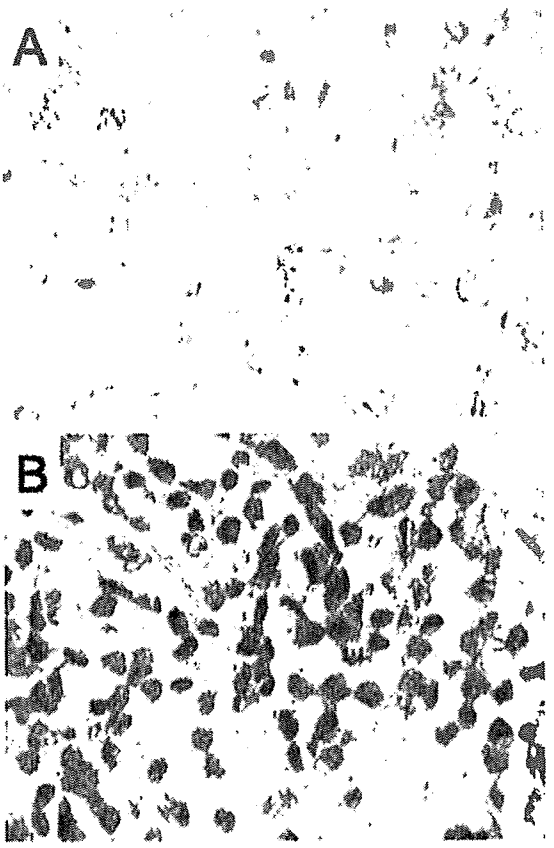

FIGURE 3 Immunohistochemical detection of WT1. Tissues were stained with anti-WT1 antibody 6F-H2 (A). WT1 protein was stained brown. The sections were then counterstained with hematoxylin (B).

CTLs can be phenotypically classified into 4 differentiation stages according to their expression of CD45RA and CCR7: naïve ($CD45RA^+CCR7^+$), central memory ($CD45R^-CCR7^+$), effector memory ($CD45RA^-CCR7^-$), and effector ($CD45RA^+CCR7^-$). Before vaccination, approximately half of $tetramer^+CD8^+$ T cells had an effector memory or effector phenotype, and these cells are considered to attack cancer cells quickly upon antigen-stimulation (Figure 4). This subset composition did not change substantially during vaccination. Compared to peripheral blood of healthy donors, in which the majority (about 80%) of $tetramer^+CD8^+$ T cells belonged to naïve phenotype [13], a high proportion of WT1-specific CTLs in peripheral blood of our patient were in an activated or differentiated stage.

No adverse effects were observed except for local erythema at the injection sites. The patient's general condition has been good without clinical relapse during WT1 peptide vaccination. The dose of WT1 peptide vaccination was increased to 2 mg from the 64th injection according to her

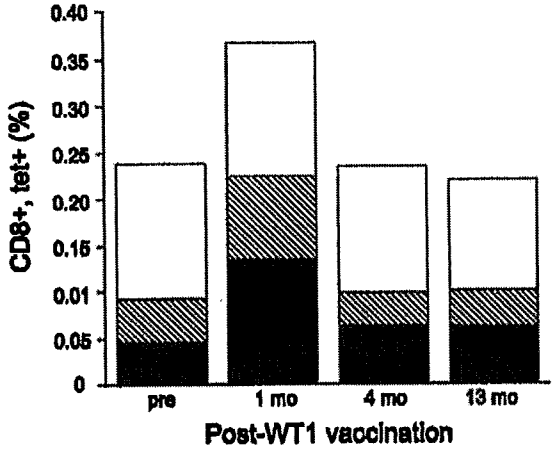

FIGURE 4 WT1-specific CTL frequencies in peripheral blood and CTLs subset composition. WT1-specific CTL frequencies are shown as percentage of WT1-tetramer$^+$CD8$^+$ T cells among CD8$^+$ T cells. CTLs were phenotypically classified into four subsets according to CD45RA and CCR7 expression: naïve (white bars), central memory (not detected), effector memory (black bars), and effector (striped bars).

weight gain. WT1 peptide vaccination has been continued to date (March 2008) without systemic adverse effects.

DISCUSSION

Rhabdomyosarcoma is the most common malignant soft tissue tumor of childhood. Patients with metastatic disease have a poor prognosis, with 5-year progression-free survival usually less than 30% [14]. Alveolar histology, confirmed by the presence of PAX3-FKHR fusion, is also associated with poor prognosis [15]. Current multidisciplinary treatment has contributed to an improvement of clinical outcomes, but control of disease is often difficult for children with metastatic alveolar rhabdomyosarcoma. Estimated 3-year event-free survival for patients with more than three metastatic sites and non-embryonal histology has been reported to be only 5% [16].

Our patient had primary disease in the lower leg with metastases on distant lymph node, bone, and bone marrow. She also developed a new metastatic bone lesion during the initial two courses of chemotherapy, indicating poor response to chemotherapy. Although she received a total of six courses of combination chemotherapy, high-dose chemotherapy, surgery on the primary site, and radiotherapy on primary and metastatic sites, bone disease remained positive. Considering her poor prognosis, we chose WT1 peptide immunotherapy. After the start of WT1 peptide immunotherapy, uptake disappeared on bone scintigraphy. Despite the resistance to initial chemotherapy, her continuing remission for more than 22 months suggests a positive effect from WT1 peptide vaccination.

The WT1 gene is physiologically expressed in some organs such as kidney, bone marrow, and pleura. Recent studies have shown that WT1-specific CTLs kill WT1-expressing tumor cells, but not normal cells. In mice immunized with MHC class I-restricted 9-mer WT1 peptides or *WT1* cDNA, WT1-specific CTLs induced killing of WT1-expressing tumor cells, but never damaged normal tissues [17, 18]. Several mechanisms have been postulated to account for WT1-specific CTLs ignoring WT1-expressing normal cells: (1) *WT1* expression levels may be different between cancer cells and normal cells; (2) mechanisms for processing of WT1 protein or presentation of WT1 peptide may be different; and (3) susceptibility of the cell membranes to CTL-producing molecules such as perforin may be different [19].

The frequency of WT1-specific CTLs is usually about 0.1% or less in healthy donors [9]. Since the frequency in our case was as high as 0.24% before WT1 peptide vaccination, this indicates that the patient had responded to the WT1 protein derived from the tumor cells and elicited WT1-specific CTLs before WT1 peptide vaccination. The frequency increased from 0.24% before vaccination to 0.37% at 1 month after starting the vaccination (1.54-fold increase). We have previously demonstrated that the emergence of clinical responses is correlated with a greater than 1.5-fold increase in tetramer$^+$ cell frequencies [9]. This finding strongly suggested that WT1 vaccination-driven induction of WT1-specific CTL responses led to a clinical effect in responders. This observation was also in line with the present case in which a greater than 1.5-fold increase in tetramer$^+$ cell frequency was observed with clinical response. Although the frequency decreased to the pre-vaccination level at 4 and 13 months, levels were maintained higher than those in healthy donors. The reason for the decrease in frequencies at later points might be explained by several mechanisms, e.g., activation-induced cell death of WT1-specific CTLs, migration of the CTLs to a tumor site, reduced stimulation of the immune system by WT1 protein owing to reduction in tumor burden (achievement of complete response). We also analyzed phenotype to evaluate the differentiation state of WT1-specific CTLs in our patient. Analysis revealed that many of the tetramer$^+$ cells had the phenotype of effector memory or effector cells, which are considered to be ready for cancer cell attack upon antigen stimulation. Taken together, the high frequencies of WT1-specific CTLs, their increase in frequency after vaccination, and the differentiated (functionally matured) state of the CTLs may contribute to the induction of clinical response.

In conclusion, WT1-peptide immunotherapy was effective with immunological response against residual disease in a child with metastatic alveolar rhabdomyosarcoma. WT1 peptide-based immunotherapy should be considered as a promising option for high-risk rhabdomyosarcoma in childhood.

Declaration of Interest: The authors report no conflicts of interest. The authors alone are responsible for the content and writing of the paper.

REFERENCES

[1] Menke AL, van der Eb AJ, Jochemsen AG. The Wilms' tumor 1 gene: Oncogene or tumor suppressor gene?. *Int Rev Cytol.* 1998;181:151–212.

[2] Ojiy , Ogawa H, Tamaki H, et al. Expression of the Wilms' tumor gene WT1 in solid tumors and its involvement in tumor cell growth. *Jpn J Cancer Res.* 1999;90:194–204.

[3] Yamagami T, Sugiyama H, Inoue K, et al. Growth inhibition of human leukemic cells by WT1 (Wilms tumor gene) antisense oligodeoxynucleotides: Implications for the involvement of WT1 in leukemogenesis. *Blood.* 1996;87:2878–2884.

[4] Inoue K, Ogawa H, Yamagami T, et al. Long-term follow-up of minimal residual disease in leukemia patients by monitoring WT1 (Wilms tumor gene) expression levels. *Blood.* 1996;88:2267–2278.

[5] Miyoshi Y, Ando A, Egawa C, et al. High expression of Wilms' tumor suppressor gene predicts poor prognosis in breast cancer patients. *Clin Cancer Res.* 2002;8:1167–1171.

[6] Nakatsuka S, Oji Y, Horiuchi T, et al. Immunohistochemical detection of WT1 protein in a variety of cancer cells. *Mod Pathol.* 2006;19:804–814.

[7] Oka Y, Tsuboi A, Murakami M, et al. Wilms tumor gene peptide-based immunotherapy for patients with overt leukemia from myelodysplastic syndrome (MDS) or MDS with myelofibrosis. *Int J Hematol.* 2003;78:56–61.

[8] Tsuboi A, Oka Y, Osaki T, et al. WT1 peptide-based immunotherapy for patients with lung cancer: Report of two cases. *Microbiol Immunol.* 2004;48:175–184.

[9] Oka Y, Tsuboi A, Taguchi T, et al. Induction of WT1 (Wilms' tumor gene)-specific cytotoxic T lymphocytes by WT1 peptide vaccine and the resultant cancer regression. *Proc Natl Acad Sci U S A.* 2004;101:13885–13890.

[10] Izumoto S, Tsuboi A, Oka Y, et al. Phase II clinical tial of Wilms tumor 1 peptide vaccination for patients with recurrent glioblastoma multiforme. *J Neurosurg.* 2008;108:963–971.

[11] Tsuboi A, Oka Y, Udaka K, et al. Enhanced induction of human WT1-specific cytotoxic T lymphocytes with a 9-mer WT1 peptide modified at HLA-A*2402-binding residues. *Cancer Immunol Immunother.* 2002;51:614–620.

[12] Wang F, Bade E, Kuniyoshi C, et al. Phase I trial of a MART-1 peptide vaccine with incomplete Freund's adjuvant for resected high-risk melanoma. *Clin Cancer Res.* 1999;5:2756–2765.

[13] Kawakami M, Oka Y, Tsuboi A, et al. Clinical and immunologic responses to very low-dose vaccination with WT1 peptide (5 microg/body) in a patient with chronic myelomonocytic leukemia. *Int J Hematol.* 2007;85:426–429.

[14] Crist W, Gehan EA, Ragab AH, et al. The Third Intergroup Rhabdomyosarcoma Study. *J Clin Oncol.* 1995;13:610–630.

[15] Sotensen PH, Lynch JC, Qualman SJ, et al. PAX3-FKHP and PAX7-FKHR gene fusions are prognostic indicators in alveolat rhabdomyosarcoma: A report from the children's oncology group. *J Clin Oncol.* 2002;20:2672–2679.

[16] Breneman JC, Lyden E, Pappo AS, et al. Prognostic factors and clinical outcomes in children and adolescents with metastatic rhabdomyosarcoma: A report from the Intergroup Rhabdomyosarcoma Study IV. *J Clin Oncol.* 2003;21:78–84.

[17] Oka Y, Udaka K, Tsuboi A, et al. Cancer immunotherapy targeting Wilms' tumor gene WT1 product. *J Immunol.* 2000;164:1873–1880.

[18] Tsuboi A, Oka Y, Ogawa H, et al. Cytotoxic T-lymphocyte responses elicited to Wilms' tumor gene WT1 product by DNA vaccination. *J Clin Immunol.* 2000;20:195–202.

[19] Oka Y, Tsuboi A, Elisseeva OA, et al. WT1 peptide cancer vaccine for patients with hematopoietic malignancies and solid cancers. *Scientific World Journal.* 2007;7:649–665.

ANTICANCER RESEARCH *29*: 1691-1696 (2009)

Immunohistochemical Detection of WT1 Protein in Endometrial Cancer

SATOSHI OHNO[1,2,3], SATOSHI DOHI[1], YUMIKO OHNO[1], SATORU KYO[1], HARUO SUGIYAMA[4], NOBUTAKA SUZUKI[1,2] and MASAKI INOUE[2]

Departments of [1]Obstetrics and Gynecology, and [2]Complementary and Alternative Medicine Clinical R&D, Kanazawa University, Graduate School of Medical Science, Ishikawa; [3]International Research and Educational Institute for Integrated Medical Science, Tokyo Women's Medical University, Tokyo; [4]Department of Functional Diagnostic Science, Osaka University, Graduate School of Medicine, Osaka, Japan

Abstract. *Background: The Wilms' tumor gene WT1 is overexpressed in various kinds of solid tumors. However, it remains unclear whether WT1 plays a pathophysiological role in endometrial cancer. Patients and Methods: A series of 70 endometrial cancer patients who had undergone a curative resection was studied to determine the correlation between WT1 expression, clinicopathological characteristics and prognosis. Tissue specimens were evaluated for WT1 expression by immunohistochemistry. Results: The expression of WT1 was strong in 31 patients (44%) and weak in 39 patients (56%). WT1 overexpression was associated with advanced FIGO stage (p=0.0266), myometrial invasion (p=0.0477) and high-grade histological differentiation (p=0.0049). The expression level of WT1 was found to be a significant predictor of disease relapse in univariate analysis (p=0.0233), but not in multivariate analysis (p=0.4757). Conclusion: These results suggested that tumor-produced WT1 provided additional prognostic information in endometrial cancer patients.*

Endometrial cancer is the most common gynecological malignancy in the United States. In Japan, it is the second most common gynecological cancer, but its frequency has dramatically increased in the last decade. Although there are well-established surgical and chemotherapeutic treatments for endometrial cancer, the need for molecular-target therapy has increased, especially for recurrent disease that has acquired radio- or chemoresistance, thus, there is a need for a better understanding of the molecular pathways of endometrial carcinogenesis.

The Wilms' tumor gene *WT1* was isolated as a gene responsible for a childhood renal neoplasm, Wilms' tumor (1, 2). This gene encodes a zinc finger transcription factor and play important roles in cell growth and differentiation (3, 4). Although *WT1* gene was categorized at first as a tumor-suppressor gene, it was recently demonstrated that the wild-type *WT1* gene performed an oncogenic rather than a tumor-suppressor function in many kinds of malignancies (5). *WT1* gene is highly expressed in hematological malignancies and solid tumors, including endometrial cancer (6). However, it remains unclear whether *WT1* plays a pathophysiological role in endometrial cancer.

Therefore, in the present study, we immunohistochemically analyzed the expression of WT1 protein in 70 cases of primary endometrial cancer to study the relationship between WT1 expression and clinicopathological characteristics as well as prognosis to clarify the prognostic significance of WT1 protein expression in endometrial cancer patients.

Patients and Methods

Patients. This study included 70 primary endometrial carcinoma patients who had been consecutively admitted, treated and followed-up at the Department of Obstetrics and Gynecology, Kanazawa University Hospital from January 1995 to December 2002. None of the patients had received any pre-surgical treatment and all had undergone a total abdominal or radical hysterectomy plus bilateral salphingo-oophorectomy. At the time of laparotomy, peritoneal fluid samples were obtained for cytological testing. Systemic pelvic lymphadenectomy was performed in 51 (72.9%) patients. Paraaortic lymph node sampling was performed in two patients because of visible or palpable enlarged lymph nodes. All the patients were classified by the International Federation of Gynecology and Obstetrics (FIGO) surgical staging system (1988). No patient had remaining macroscopic tumors or known distant metastasis immediately after surgery. The high-risk patients (*e.g.* these with deep myometrial invasion, cervical involvement, special histology,

Correspondence to: Satoshi Ohno, Department of Complementary and Alternative Medicine Clinical R&D, Kanazawa University, Graduate School of Medical Science, 13-1 Takaramachi, Kanazawa, Ishikawa, 920-8640 Japan. Tel: +81 762652147, Fax: +81 762344247, e-mail: satoshi.ohno55@gmail.com

Key Words: WT1, immunohistochemistry, endometrial cancer, clinicopathological factors, prognosis.

0250-7005/2009 $2.00+.40

or peritoneal cytology) underwent external radiotherapy and/or six cycles of chemotherapy (paclitaxel: 180 mg/m^2, carboplatin: according to Chatelut's formula [AUC=5 mg min/ml]) as postoperative adjuvant therapy.

The treatment was followed by a gynecological examination, recording of laboratory data, transvaginal/abdominopelvic ultrasonography and a radiological investigation. The data from regular follow-up visits to the outpatient department were stored in a database specifically designed for endometrial carcinoma patients. A telephone inquiry to update the present status of all surviving patients was made in August 2006. The exact date of disease recurrence was obtained from the referring physicians or from the physicians who attended the patient for the initial diagnosis of the recurrence. All the treatments and clinical research were conducted with written informed consent.

Immunohistochemistry. Formalin-fixed and paraffin-embedded tissues from 70 tumors were retrieved with informed consent from archive sources at Kanazawa University Hospital. The histological diagnosis of each tumor was confirmed on the hematoxylin and eosin-stained sections. Representative sections containing both the normal endometrium and the invasive front of the tumor tissue were selected for immunohistochemical staining. The slides were deparaffinized and rehydrated in graded alcohols. Epitope retrieval was performed using enzymatic digestion with Proteinase K for 30 minutes at 37°C (Dako Cytomation, Carpinteria, CA, USA), and by microwave heating for 15 minutes using Target Retrieval Solution (Dako Cytomation). Endogenous peroxidase activity was quenched by dipping in 3% hydrogen peroxide for 30 minutes. The slides were incubated with mouse monoclonal antibodies (clone 6F-H2; Dako Cytomation) diluted 1:100 at 4°C overnight. The subsequent steps were carried out according to the manufacturer's instructions by the EnVision+ ® System horseradish peroxidase (HRP)-labelled polymer (Dako Cytomation). Color development was carried out with peroxidase substrate 3-amino-9-ethylcarbazole (AEC). All the slides were counterstained with Mayer's hematoxylin. Formalin-fixed, paraffin-embedded sections of human Wilms' tumor were used as positive controls for WT1.

Evaluation of staining. For evaluation of WT1 expression, staining intensity was scored as 0 (negative), 1 (weak), 2 (medium) and 3 (strong). The extent of staining was scored as 0 (0%), 1 (1-25%), 2 (26-50%), 3 (51-75%) and 4 (76-100%) according to the percentage of the positive staining area in relation to the whole carcinoma area. The sum of the intensity and extent score was used as the final staining score (0-7) for WT1. Tumors having a final staining score of ≥5 were considered to exhibit strong expression. All the histological slides were examined by two observers (S.O. and Y.O.) who were unaware of the clinical data or the disease outcome.

Statistical analysis. The Chi-square test for 2×2 tables was used to compare the categorical data. Mortality and probability of relapse after surgery were compared by Kaplan-Meier analysis and the log-rank statistic. In the analysis of relapse-free survival rates, those who died of causes unrelated to endometrial cancer and those who had no detected evidence of disease recurrence were considered to be relapse-free. A p-value of <0.05 was considered to indicate statistical significance. All the statistical analyses were performed using the statistical package StatView version 5.0 for Macintosh (Abacus Concepts, Berkeley, CA, USA).

Results

Characteristics of the patients. The patients' average age at the time of surgery was 57.3 years (range, 26-78 years), 22 had premenopausal status, 4 had perimenopausal status and 44 had postmenopausal status. The patients' mean preoperative body mass index (BMI) was 24.0 (range, 16.9-32.9). Among the 70 patients, 12 patients (17.1%) had relapses of endometrial cancer at the time of the last follow-up. The median follow-up time for all the patients was 5.12 years (range, 0.56-11.08 years).

WT1 expression in endometrial cancer. WT1 expression was positive exclusively in cancer cells in 64 cases (91%). The expression of WT1 was strong (final staining score of 5-7) in 31 patients (44%) and weak (final staining score of 0-4) in 39 patients (56%). The typical WT1 expression in endometrial cancer cells is shown in Figure 1. A majority of the positive cases showed diffuse or granular staining in the cytoplasm. The staining of WT1 was heterogeneous in advanced tumors and WT1 was frequently located at the invasion front of the tumor. The association between WT1 expression and clinicopathological variables is shown in Table I. WT1 overexpression was associated with advanced FIGO stage (p=0.0266), myometrial invasion (p=0.0477) and high-grade histological differentiation (p=0.0049), indicating up-regulation of WT1 expression with tumor progression in this study.

Prognostic impact of WT1 expression in endometrial cancer. Strong expression of WT1 was associated with reduced relapse-free survival in endometrial cancer (Figure 2A). Although there was no clear statistical significance, WT1 expression was a factor negatively influencing the overall survival rate (Figure 2B). Multivariate analysis indicated that WT1 expression had no independent significant effect (data not shown).

Discussion

With the use of anti-WT1 monoclonal (6F-H2) antibody, positive staining in the tumor cells was observed in 91% of the cases. The relatively high rate of positivity for WT1 in the present study contrasts with some previous reports. Acs *et al.* (7) reported that WT1 immunoreactivity was seen in ten of 16 serous, but in none of 35 endometrioid or 18 clear cell carcinomas among endometrial carcinomas. Egan *et al.* (8) also reported that two of 31 serous carcinomas and none of 39 endometrioid carcinomas were reactive for WT1. Meanwhile, Dupont *et al.* (9) confirmed that WT1 expression was found in twenty of 99 endometrioid carcinomas using polyclonal antibody against WT1 (Santa Cruz; clone C-19). The discrepancy between our findings and previous results could be explained by the different criteria employed to judge WT1 positivity: they regarded nuclear but not cytoplasmic

Figure 1. *Representative sections of endometrial cancer with immunohistochemical staining of WT1. Strong cytoplasmic staining is observed in the invasion front of the tumor (×40; inset, ×200).*

staining in the tumor cells as positive, because WT1 is principally a DNA-binding transcription factor mainly distributed in the nucleus. In the present study, granular or diffuse cytoplasmic staining in the tumor cells was judged as positive, for reasons explained below.

Nakatsuka *et al.* reported that Western blot analysis revealed the intracytoplasmic localization of WT1 protein in lung cancer cells (6). Oji *et al.* (10) and Drakos *et al.* (11) showed the cytoplasmic expression of WT1 protein in cell lines derived from glioblastoma and lymphoma. Moreover, Ye *et al.* (12) revealed that phosphorylation in the DNA-binding domain of WT1 alters the affinity for DNA and subcellular distribution of WT1. Post-translational phosphorylation at zinc fingers inhibits the ability to bind DNA, resulting in the cytoplasmic retention of WT1, and also inhibits transcriptional regulatory activity. As established by the interesting study of Niksic *et al.* (13), WT1 shuttles between the nucleus and cytoplasm and might be involved in the regulation of translation through its association with actively translating polysomes. Recent studies found that many types of tumor frequently showed strong cytoplasmic expression of WT1, suggesting that WT1 was involved in the development of tumors (6, 10, 14-16). In the present study, we also found that the majority of endometrial tumors showed strong cytoplasmic WT1 staining, which was associated with advanced FIGO stage, myometrial invasion and high-grade histological differentiation. These results suggest that up-regulation of WT1 expression is linked to tumor progression.

To date, few reports are available on the prognostic impact of WT1 expression in endometrial cancer patients. Miyoshi *et al.* (17) reported that the disease-free survival rate was significantly lower in breast cancer patients with high levels of *WT1* mRNA than those with low levels. Inoue *et al.* (18) showed that leukemia with strong *WT1* mRNA expression

Table I. *WT1 expression and clinicopathological characteristics.*

Variable	WT1 expression		*P*-value (χ^2 test)
	Strong (n=31)	Weak (n=39)	
Age (year)			
<60 (n=43)	16	27	
≥60 (n=27)	15	12	0.1325
FIGO stage			
I (n=52)	19	33	
II, III, IV (n=18)	12	6	0.0266
Lymph node metastasis			
Negative (n=65)	28	37	
Positive (n=5)	3	2	0.4629
Depth (myometrial invasion)			
a (n=17)	4	13	
b, c (b, n=36; c, n=17)	27	26	0.0477
Histopathology-degree of differentiation			
Grade 1 (n=38)	11	27	
Grade 2, 3 (n=32)	20	12	0.0049
Menopause			
Peri, pre (n=26)	8	18	
Post (n=44)	23	21	0.0801
Body mass index			
<25 (n=45)	19	26	
≥25 (n=25)	12	13	0.6410

showed a significantly lower rate of complete remission and significantly worse overall survival than that with weak expression. Moreover, Sera *et al.* (19) reported that overexpressed WT1 protein, which was confirmed by Western blotting and immunohistochemical staining, was an independent prognostic factor for disease-free survival in hepatocellular carcinoma patients. Høgdall *et al.* (20) demonstrated that univariate Kaplan-Meier survival analysis performed on 560 ovarian cancer patients showed a significantly shorter disease-specific survival in patients with positive WT1 protein expression in the tumor tissue. Netinatsunthorn *et al.* (21) also reported that immunohistochemical expression of WT1 was a prognostic predictor in patients with advanced serous epithelial ovarian carcinoma. In the present study, we found that strong expression of WT1 was associated with reduced relapse-free survival in endometrial cancer patients. Our results are congruent with previous reports of other types of cancer.

WT1 could be a novel tumor rejection antigen in immunotherapy for various kinds of WT1-expressing cancer. Clinical trials of WT1 peptide-based cancer immunotherapy showed that WT1 vaccination induced a reduction in tumor size or decrease in tumor marker levels in breast, lung cancer, leukemia and glioblastoma multiforme (22, 23). The results of the present study provide a rationale for immunotherapy targeting WT1 as a new treatment strategy for endometrial cancer.

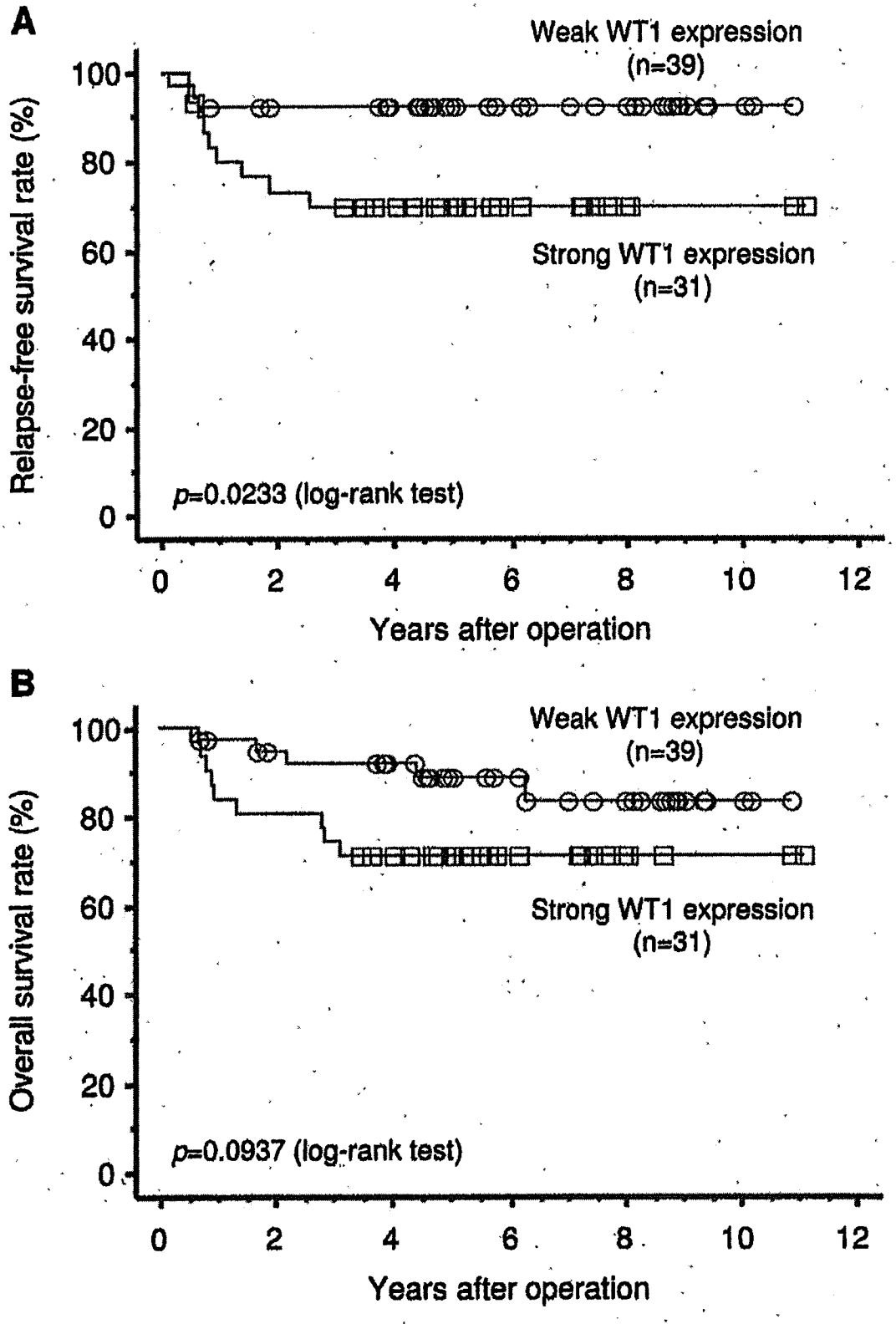

Figure 2. *The Kaplan-Meier survival curves of 70 patients with endometrial carcinoma in relation to WT1 expression are shown. A, Relapse-free survival rate; B, overall survival rate.*

In conclusion, our study now shows the cytoplasmic expression of WT1 might provide additional prognostic information for endometrial cancer patients.

Acknowledgements

This work was supported by a Grant-in-Aid for Young Scientists (B) (No. 19791140) from the Ministry of Education, Culture, Sports, Science and Technology of the Japanese Government. We are grateful to the staff at the Pathology Section, Kanazawa University Hospital, for collecting the samples and providing paraffin-embedded tissues. We also thank Ms. Tokiko Hakamata (Kanazawa University) for technical assistance.

References

1 Call KM, Glaser T, Ito CY, Buckler AJ, Pelletier J, Haber DA, Rose EA, Kral A, Yeger H, Lewis WH, Jones C and Housman DE: Isolation and characterization of a zinc finger polypeptide gene at the human chromosome 11 Wilms' tumor locus. Cell *60*: 509-520, 1990.

2 Gessler M, Poustka A, Cavenee W, Neve RL, Orkin SH and Bruns GA: Homozygous deletion in Wilms tumours of a zinc-finger gene identified by chromosome jumping. Nature *343*: 774-778, 1990.

3 Sugiyama H: Wilms' tumor gene *WT1*: its oncogenic function and clinical application. Int J Hematol *73*: 177-187, 2001.

4 Oka Y, Tsuboi A, Kawakami M, Elisseeva OA, Nakajima H, Udaka K, Kawase I, Oji Y and Sugiyama H: Development of WT1 peptide cancer vaccine against hematopoietic malignancies and solid cancers. Curr Med Chem *13*: 2345-2352, 2006.

5 Yang L, Han Y, Suarez Saiz F and Minden MD: A tumor suppressor and oncogene: the WT1 story. Leukemia *21*: 868-876, 2007.

6 Nakatsuka S, Oji Y, Horiuchi T, Kanda T, Kitagawa M, Takeuchi T, Kawano K, Kuwae Y, Yamauchi A, Okumura M, Kitamura Y, Oka Y, Kawase I, Sugiyama H and Aozasa K: Immunohistochemical detection of WT1 protein in a variety of cancer cells. Mod Pathol *19*: 804-814, 2006.

7 Acs G, Pasha T and Zhang PJ: WT1 is differentially expressed in serous, endometrioid, clear cell, and mucinous carcinomas of the peritoneum, fallopian tube, ovary, and endometrium. Int J Gynecol Pathol *23*: 110-118, 2004.

8 Egan JA, Ionescu MC, Eapen E, Jones JG and Marshall DS: Differential expression of WT1 and p53 in serous and endometrioid carcinomas of the endometrium. Int J Gynecol Pathol *23*: 119-122, 2004.

9 Dupont J, Wang X, Marshall DS, Leitao M, Hedvat CV, Hummer A, Thaler H, O'Reilly RJ and Soslow RA: Wilms tumor gene (*WT1*) and p53 expression in endometrial carcinomas: a study of 130 cases using a tissue microarray. Gynecol Oncol *94*: 449-455, 2004.

10 Oji Y, Suzuki T, Nakano Y, Maruno M, Nakatsuka S, Jomgeow T, Abeno S, Tatsumi N, Yokota A, Aoyagi S, Nakazawa T, Ito K, Kanato K, Shirakata T, Nishida S, Hosen N, Kawakami M, Tsuboi A, Oka Y, Aozasa K, Yoshimine T and Sugiyama H: Overexpression of the Wilms' tumor gene *WT1* in primary astrocytic tumors. Cancer Sci *95*: 822-827, 2004.

11 Drakos E, Rassidakis GZ, Tsioli P, Lai R, Jones D and Medeiros LJ: Differential expression of *WT1* gene product in non-Hodgkin lymphomas. Appl Immunohistochem Mol Morphol *13*: 132-137, 2005.

12 Ye Y, Raychaudhuri B, Gurney A, Campbell CE and Williams BR: Regulation of WT1 by phosphorylation: inhibition of DNA binding, alteration of transcriptional activity and cellular translocation. EMBO J *15*: 5606-5615, 1996.

13 Niksic M, Slight J, Sanford JR, Caceres JF and Hastie ND: The Wilms' tumour protein (WT1) shuttles between nucleus and cytoplasm and is present in functional polysomes. Hum Mol Genet *13*: 463-471, 2004.

14 Nakahara Y, Okamoto H, Mineta T and Tabuchi K: Expression of the Wilms' tumor gene product WT1 in glioblastomas and medulloblastomas. Brain Tumor Pathol *21*: 113-116, 2004.

15 Carpentieri DF, Nichols K, Chou PM, Matthews M, Pawel B and Huff D: The expression of WT1 in the differentiation of rhabdomyosarcoma from other pediatric small round blue cell tumors. Mod Pathol *15*: 1080-1086, 2002.

16 Sebire NJ, Gibson S, Rampling D, Williams S, Malone M and Ramsay AD: Immunohistochemical findings in embryonal small round cell tumors with molecular diagnostic confirmation. Appl Immunohistochem Mol Morphol *13*: 1-5, 2005.

17 Miyoshi Y, Ando A, Egawa C, Taguchi T, Tamaki Y, Tamaki H, Sugiyama H and Noguchi S: High expression of Wilms' tumor suppressor gene predicts poor prognosis in breast cancer patients. Clin Cancer Res *8*: 1167-1171, 2002.

18 Inoue K, Sugiyama H, Ogawa H, Nakagawa M, Yamagami T, Miwa H, Kita K, Hiraoka A, Masaoka T, Nasu K, Kyo T, Dohy H, Nakauchi H, Ishidate T, Akiyama T and Kishimono T: WT1 as a new prognostic factor and a new marker for the detection of minimal residual disease in acute leukemia. Blood *84*: 3071-3079, 1994.

19 Sera T, Hiasa Y, Mashiba T, Tokumoto Y, Hirooka M, Konishi I, Matsuura B, Michitaka K, Udaka K and Onji M: *Wilms' tumour 1* gene expression is increased in hepatocellular carcinoma and associated with poor prognosis. Eur J Cancer *44*: 600-608, 2008.

20 Høgdall EV, Christensen L, Kjaer SK, Blaakaer J, Christensen IJ, Gayther S, Jacobs IJ and Høgdall CK: Expression level of Wilms tumor 1 (WT1) protein has limited prognostic value in epithelial ovarian cancer: from the Danish "MALOVA" ovarian cancer study. Gynecol Oncol *106*: 318-324, 2007.

21 Netinatsunthorn W, Hanprasertpong J, Dechsukhum C, Leetanaporn R and Geater A: *WT1* gene expression as a prognostic marker in advanced serous epithelial ovarian carcinoma: an immunohistochemical study. BMC Cancer *6*: 90-98, 2006.

22 Oka Y, Tsuboi A, Taguchi T, Osaki T, Kyo T, Nakajima H, Elisseeva OA, Oji Y, Kawakami M, Ikegame K, Hosen N, Yoshihara S, Wu F, Fujiki F, Murakami M, Masuda T, Nishida S, Shirakata T, Nakatsuka S, Sasaki A, Udaka K, Dohy H, Aozasa K, Noguchi S, Kawase I and Sugiyama H: Induction of *WT1* (Wilms' tumor gene)-specific cytotoxic T lymphocytes by WT1 peptide vaccine and the resultant cancer regression. Proc Natl Acad Sci USA *101*: 13885-13890, 2004.

23 Izumoto S, Tsuboi A, Oka Y, Suzuki T, Hashiba T, Kagawa N, Hashimoto N, Maruno M, Elisseeva OA, Shirakata T, Kawakami M, Oji Y, Nishida S, Ohno S, Kawase I, Hatazawa J, Nakatsuka S, Aozasa K, Morita S, Sakamoto J, Sugiyama H and Yoshimine T: Phase II clinical trial of Wilms tumor 1 peptide vaccination for patients with recurrent glioblastoma multiforme. J Neurosurg *108*: 963-971, 2008.

Received August 19, 2008
Revised December 11, 2008
Accepted February 13, 2009

Clinical Neurology and Neurosurgery 111 (2009) 527–535

Contents lists available at ScienceDirect

Clinical Neurology and Neurosurgery

journal homepage: www.elsevier.com/locate/clineuro

Spectroscopy-supported frame-based image-guided stereotactic biopsy of parenchymal brain lesions: Comparative evaluation of diagnostic yield and diagnostic accuracy

Mikhail F. Chernov[a,b,d,*], Yoshihiro Muragaki[b,d], Taku Ochiai[b], Takaomi Taira[b], Yuko Ono[c], Masao Usukura[c], Takashi Maruyama[b,d], Kotaro Nakaya[b], Ryoichi Nakamura[a,d], Hiroshi Iseki[a,b,d], Osami Kubo[b], Tomokatsu Hori[b], Kintomo Takakura[a,b,d]

[a] International Research and Educational Institute for Integrated Medical Sciences (IREIIMS), Tokyo Women's Medical University, Tokyo, Japan
[b] Department of Neurosurgery, Neurological Institute, Tokyo Women's Medical University, Tokyo, Japan
[c] Department of Neuroradiology, Neurological Institute, Tokyo Women's Medical University, Tokyo, Japan
[d] Faculty of Advanced Techno-Surgery, Institute of Advanced Biomedical Engineering and Science, Tokyo Women's Medical University, Tokyo, Japan

ARTICLE INFO

Article history:
Received 7 October 2008
Received in revised form 16 March 2009
Accepted 20 March 2009

Keywords:
Brain tumor
Stereotactic biopsy
Diagnostic yield
Diagnostic accuracy
Metabolic imaging
Proton magnetic resonance spectroscopy

ABSTRACT

Objective: Comparative evaluation of diagnostic efficacy of stereotactic brain biopsy performed with and without additional use of spectroscopic imaging (^{1}H-MRS) for target selection was done.
Methods: From 2002 to 2006, 30 patients with parenchymal brain lesions underwent ^{1}H-MRS-supported frame-based stereotactic biopsy, whereas in 39 others MRI-guided technique was used. Comparison of diagnostic yield of the procedure in these two groups was performed. Additionally, the diagnostic accuracy was evaluated in 37 lesions, which were surgically resected within 1 month thereafter.
Results: Stereotactic biopsy permitted establishment of a definitive histopathological diagnosis in 57 cases and diagnosis of low-grade glioma without specific tumor typing in 8 cases. In 4 cases tissue sampling was non-diagnostic. In 5 out of 8 cases with incomplete diagnosis and in all non-diagnostic cases target selection was performed without the use of ^{1}H-MRS ($P=0.2073$). The diagnostic yields of ^{1}H-MRS-supported and MRI-guided procedures were 100% and 90%, respectively ($P=0.1268$). Comparison of the histopathological diagnoses after stereotactic biopsy and surgical resection revealed complete diagnostic agreement in 13 cases, minor disagreement in 14 cases, and major disagreement in 10 cases. Among these last 10 cases, initial undergrading of non-enhancing WHO grade III gliomas was the most common (7 cases). The diagnostic accuracy of ^{1}H-MRS-supported and MRI-guided procedures was 67% and 79%, respectively ($P=0.4756$).
Conclusion: While in the present study the diagnostic yield of ^{1}H-MRS-supported frame-based stereotactic brain biopsy was 100%, its statistically significant diagnostic advantages over MRI-guided technique were not proved. Optimal selection of the spectroscopic target for tissue sampling remains unclear.

1. Introduction

Minimally invasive image-guided stereotactic biopsy is a routine neurosurgical procedure that provides an excellent opportunity to establish histopathological diagnosis of parenchymal brain lesions in virtually any location. Introduction of modern neuroimaging and development of computer-based techniques significantly facilitated target selection and navigation during tissue sampling. Nevertheless, from 0.8% to 18.6% of stereotactic biopsies are considered non-diagnostic [1–14]. Moreover, even if histopathological diagnosis is provided, it can significantly differ from that determined after subsequent lesion resection. The rate of such discrepancy varies widely, from 3% to 49% [2,7,11,15–18].

The specific cause of diagnostic failure of stereotactic brain biopsy is the limitation of the structural neuroimaging in the evaluation of the lesion heterogeneity and subsequent suboptimal tissue sampling [8,19–26]. The use of metabolic information provided by positron emission tomography (PET) [18,19,22,24,27–33], single photon emission computed tomography (SPECT) [34], and spectroscopic imaging [20,35–45] for target selection can potentially result in improved diagnostic efficacy of the procedure. However, this has not been investigated in any controlled study. The objective of the present analysis was comparative evaluation of both

* Corresponding author at: International Research and Educational Institute for Integrated Medical Sciences (IREIIMS), Tokyo Women's Medical University, 8-1 Kawada-cho, Shinjuku-ku, Tokyo 162-8666, Japan. Tel.: +81 3 3353 8111x66003; fax: +81 3 5312 1844.
E-mail address: m_chernov@yahoo.com (M.F. Chernov).

0303-8467/$ – see front matter © 2009 Elsevier B.V. All rights reserved.
doi:10.1016/j.clineuro.2009.03.006

diagnostic yield and diagnostic accuracy of the frame-based image-guided stereotactic biopsy of parenchymal brain lesions performed with and without additional use of metabolic data obtained with multivoxel proton magnetic resonance spectroscopy (^{1}H-MRS).

2. Materials and methods

From January 1, 2002 to December 31, 2006, 69 consecutive frame-based image-guided stereotactic biopsies of parenchymal brain lesions were performed in the Department of Neurosurgery of the Tokyo Women's Medical University. In 30 cases ^{1}H-MRS-detected metabolic information was used during target selection, whereas in 39 cases MRI-guided technique was utilized. The method of target selection (with or without the use of spectroscopic imaging) was determined by treating neurosurgeon according to his/her own preference, and no attempt of randomization was made. In both groups of patients, stereotactic biopsy was performed by two neurosurgeons (Drs. T. Ochiai and T. Taira), whereas tumor resection was done by three others (Drs. Y. Muragaki, T. Maruyama, and T. Hori).

One patient underwent stereotactic biopsy twice with an interval of 6 months, which was considered to be two separate cases. Low-grade astrocytoma was diagnosed after the initial MRI-guided procedure. The patient was followed without treatment, but due to rapid tumor progression the tissue sampling was repeated using ^{1}H-MRS support for target selection. At that time the diagnosis of glioblastoma was established. Another patient underwent a course of fractionated radiation therapy (total dose, 50 Gy) for suspected pontine glioma 15 months before stereotactic biopsy. All of the 66 other lesions were either previously untreated or unresponsive to conventional medical therapy, including steroids.

All data for the present analysis were extracted from the constantly maintained surgical, pathological, and radiological databases. For the purpose of the study all MRI and ^{1}H-MRS images were reviewed by a neurosurgeon and a neuroradiologist. Some cases from the same series had been analyzed separately and published previously elsewhere [46].

2.1. Clinical characteristics of patients

There were 45 males and 24 females. Their ages varied from 1 to 78 years (mean, 43 ± 19 years; median, 40 years). The series included 7 pediatric patients, but only one of them was less than 5 years old. According to the regulations of our hospital all patients were tested before surgery for human immunodeficiency virus (HIV), and no positive case was included in the present series.

There were 67 supratentorial and 2 infratentorial lesions. The predominant locations were the cerebral lobe (54 cases), basal ganglia and thalamus (11 cases), corpus callosum, pineal region, pons, and cerebellar hemisphere (1 case in each). Overall, 33 lesions were located on the left side, 32 on the right side, and 4 along the midline.

The majority of lesions (59 cases) had low intensity signal on T_1-weighted images, and high intensity signal on T_2-weighted images. A cyst-like structure of the lesion was noted in 3 cases only. Contrast enhancement was presented in 33 lesions, and was characterized as homogeneous in 8 cases, heterogeneous in 17, ring-like in 4, and patchy in 4.

Comparison of clinical and radiological variables in two groups of patients did not reveal statistically significant differences (Table 1).

2.2. Indications for stereotactic biopsy of parenchymal brain lesions

During the study period not more than 10% of the patients with parenchymal brain lesions underwent stereotactic biopsy in our clinic. The decision to perform tissue sampling was usually made by treating neurosurgeon and approved by the Chairman of the Department (Dr. T. Hori). The indications for the procedure included:

- clarification of the histopathological diagnosis, which could not be established based on clinical and radiological investigations, particularly for the differentiation of neoplastic and non-neoplastic lesions;
- histopathological confirmation of the diagnosis of the tumor, for which treatment with chemotherapy and/or irradiation was planned (for example, malignant lymphoma);
- stereotactic implantation of electrodes for preoperative brain mapping in the cases of gliomas; simultaneous sampling of the neoplasm was usually performed for the consideration of the rationale for its aggressive surgical resection.

Informed consent was obtained from each patient and/or his or her nearest family member. The protocol of ^{1}H-MRS-supported stereotactic brain biopsy was approved by responsible authorities of Tokyo Women's Medical University.

2.3. Neuroradiological guidance

On the day of treatment a Leksell G stereotactic frame (Elekta Instruments AB, Stockholm, Sweden) was fixed on the patient's head under local anesthesia, with the exception of a 1-year-old child, who was under general anesthesia during all stages of the procedure. Axial slices of the plain and contrast-enhanced CT, as well as axial slices of T_2-weighted MRI, and axial, coronal, and sagittal slices of T_1-weighted MRI before and after intravenous injection of single-dose (0.1 mmol/kg) gadoteridol (ProHance®; Eisai Co., Tokyo, Japan), were obtained through each 2 mm under stereotactic conditions. Cerebral angiography was performed in selected cases.

In cases of ^{1}H-MRS-supported stereotactic biopsy, a two-dimensional multivoxel long-echo (TR: 1500 ms, TE: 136 ms) volume-selected spectrum was acquired using double spin-echo acquisition mode, similar to point-resolved spectroscopy (PRESS). Axial postcontrast T_1-weighted MRI was mainly used as a scout image. Under three-dimensional control the ^{1}H-MRS voxel, separated by phase-encoding in 16 rectangular subvoxels (size 15 mm × 15 mm × 15 mm and volume 3.4 cm^3 each), was located on the maximal projection of the lesion. Spatial suppression pulses were applied to the outsides of the voxel to reduce spectral contamination. Global and localized shimming on the water proton and optimization of the water suppression were performed, resulting in water peak line widths of 2–4 Hz. Automatic spectral reconstruction with frequency referencing and application of the zero-level was achieved by software provided by the supplier (MRS-PRO/PX; Toshiba Medical Systems, Tokyo, Japan). Typically, time domain data were zero-filled to 4000 data points and multiplied with a Gaussian function, exponential line broadening was performed, two-dimensional Fourier transformation of the time domain signal into frequency domain signal was done, and baseline and zero-order phase corrections were applied. Metabolite signals from mobile lipids (Lip) [0.8 and 1.3 ppm], lactate (Lac) [1.3 ppm], N-acetylaspartate (NAA) [2.0 ppm], creatine and phosphocreatine (Cr) [3.0 ppm], and choline-containing compounds (Cho) [3.2 ppm] were obtained. Their peak intensity was calculated as an area under the curve. Thereafter, the metabolite ratio of NAA/Cho was calculated in each subvoxel and used for target selection. In the present study, the content of other identified metabolites, namely Lip, Lac, and Cr, was not taken into consideration during tissue sampling.

Both MRI and ^{1}H-MRS were acquired with a 1.5 T clinical imager (ExcellArt; Toshiba Medical Systems, Tokyo, Japan). A brain quadrature (QD) coil (Type MJQH107A-S1A; Toshiba Medical Systems)

Table 1
Clinical and radiological characteristics of cases in the present series.

Variables	All cases	Comparison of two investigated groups		
		MRI-guided technique ($N=39$)	^{1}H-MRS-supported procedures ($N=30$)	P-value
Patient age (years)				
Median	40	42	38	0.4593*
Range	1–78	1–72	12–78	
Patient gender				
Men	45	29	16	0.0688**
Women	24	10	14	
Predominant lesion location				
Cerebral Lobe	54	29	25	0.3271**
Basal ganglia/thalamus	11	7	4	
Others	4	3	1	
Lesion side				
Left	33	21	12	0.2543**
Right	32	16	16	
Midline	4	2	2	
Signal intensity of the lesion on MRI				
Typical (low on T_1; high on T_2)	59	34	25	0.6527**
Non-typical	10	5	5	
Contrast enhancement				
Yes	33	22	11	0.1031**
No	36	17	19	
Number of obtained tissue samples				
1	39	23	16	0.6384***
2	11	6	5	
3	7	2	5	
4	7	5	2	
5	2	1	1	
6	1	1	–	
7	1	1	–	
9	1	–	1	
Median	1	1	1	

N: number of cases.
* According to median test for two samples.
** According to chi-square test.
*** Comparison was done with chi-square test for cases with one vs. two and more obtained tissue samples.

was used. The spectroscopic examination usually required around 8 min.

2.4. Target selection and biopsy technique

All neuroradiological data were transferred for co-registration to Leksell GammaPlan version 2.0 or, later, Leksell SurgiPlan Release 2.20 (Elekta Instruments AB). Target selection was performed by reference to a simultaneous onscreen display of all obtained images. If biopsy was based on the structural neuroimaging alone, the contrast-enhanced part of the lesion, or its center, in cases of non-enhancing pathologies, was selected for tissue sampling. In cases of ^{1}H-MRS-supported biopsy the lesion-contained subvoxel with the lowest NAA/Cho ratio was identified and the contrast-enhanced part of the lesion within this area was selected as a target (Fig. 1). If the contrast-enhanced part of the lesion did not correspond to the ^{1}H-MRS subvoxel with the lowest NAA/Cho ratio, separate tissue specimens were obtained from each area. If contrast enhancement was absent, the center of the lesion was usually targeted, as well as the area corresponding to the ^{1}H-MRS subvoxel with the lowest NAA/Cho ratio. The actual value of the NAA/Cho ratio in the target in cases of ^{1}H-MRS-supported stereotactic biopsy varied from 0.04 to 1.38 (mean, 0.52 ± 0.37; median, 0.43).

All the procedures were performed under local anesthesia with additional intravenous sedation, except in the case of a 1-year-old child, who was operated on under general anesthesia. The supine position was used in all but one of the patients. Tissue samples were obtained with a Sedan-type blunt side-cutting aspiration biopsy needle. Each histological specimen thus obtained was divided into two parts for intraoperative and permanent histopathological investigation, respectively. If the examination of the frozen biopsy sections did not determine the type of the pathological process, the tissue sampling was usually repeated using either the same or another target. The number of biopsy samples obtained did not differ significantly between two investigated groups of patients (Table 1).

2.5. Histopathological diagnosis

Final histopathological diagnosis was established on the formalin-fixed paraffin-embedded tissue sections. It was considered to be (Table 2):

- definitive, if both type and grade of the tumor or nature of the non-neoplastic pathological process was defined;
- incomplete, if neoplastic pathology was determined, but its precise type and/or grade remained unclear;
- non-diagnostic, if histopathological findings were non-specific and did not permit establishment of a diagnosis of the lesion.

The neuropathologist was fully informed about the clinical history, radiological characteristics of the lesion, and target positioning. Grading and typing of tumors was based on the World Health Organization (WHO) criteria and was retrospectively adapted to its latest requirements [47]. For the diagnosis of oligoastrocytoma the presence of both astrocytic and oligodendroglial components should

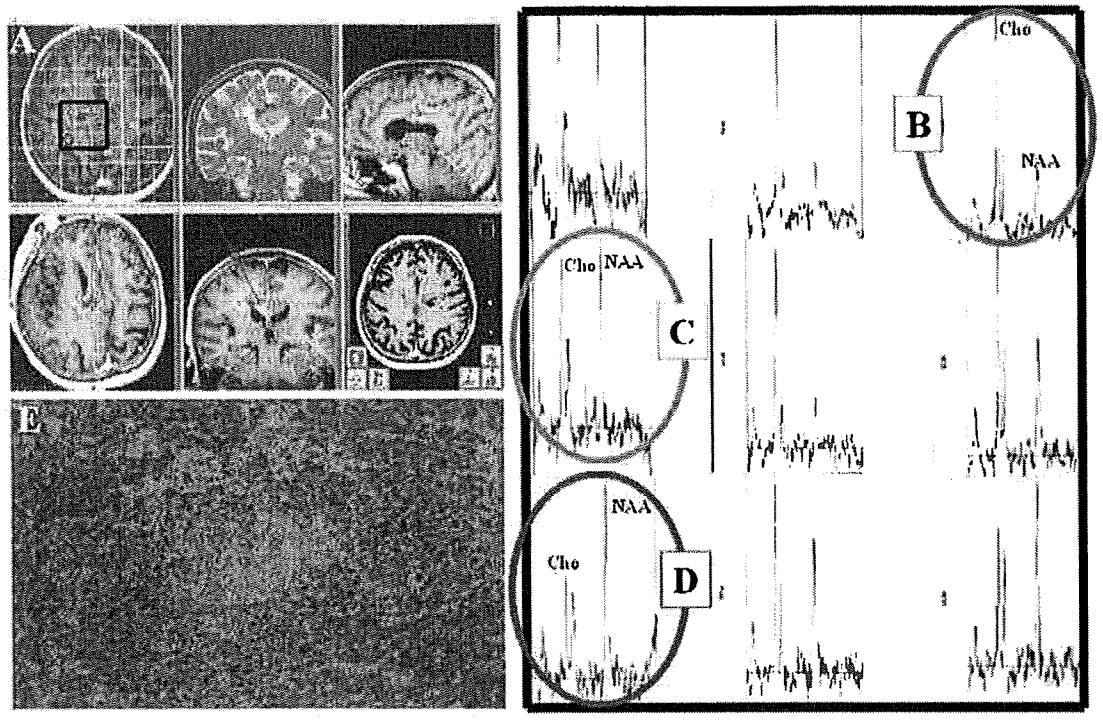

Fig. 1. Spectroscopy-supported stereotactic biopsy of the right-sided fronto-parietal tumor: ^{1}H-MRS scout image and MR images were co-registered in Leksell SurgiPlan (A), spectrum with the lowest NAA/Cho ratio (0.34) was identified (B), and contrast-enhanced part of the lesion within this area was targeted. Less significant metabolic alterations (NAA/Cho ratio 1.03) in the lesion-contained subvoxel (C) and practically normal ^{1}H-MR spectrum (NAA/Cho ratio 1.98) in the vicinity to the neoplasm (D) are shown for comparison. The histopathological examination revealed glioblastoma multiforme (E). Peaks of N-acetylaspartate (NAA) and choline-containing compounds (Cho) are marked.

constitute not less than 25% [48]; otherwise a diagnosis of glioma with specific cell component was made.

2.6. Further treatment

In 37 cases (18 after ^{1}H-MRS-supported stereotactic biopsy and 19 after MRI-guided procedures), microsurgical excision of the lesion was performed within a month (on average, in 2 ± 1 weeks) after initial tissue sampling. In the vast majority of gliomas, more than 80% resection was attained according to our policy of their aggressive surgical management [49].

Histopathological diagnosis of the lesion after craniotomy was established on the formalin-fixed paraffin-embedded tissue sections of all obtained pathological material, without specific investigation of the area sampled during initial stereotactic biopsy. Diagnostic agreement was considered as [11]:

- complete, if final histopathological diagnoses after both procedures were identical;
- minor disagreement, if final histopathological diagnoses after both procedures were slightly different, but without significant impact on the treatment strategy and prognosis;
- major disagreement, if histopathological diagnoses after both procedures differed significantly, which could have a serious impact on the choice of the appropriate management and determination of prognosis.

2.7. Statistics

The chi-square test, the median test for two samples, and Fisher's exact test were used for data analysis. The level of significance was determined at $P < 0.05$.

3. Results

3.1. Complications

One patient in the present series had an intratumoral hemorrhage immediately after stereotactic biopsy of malignant lymphoma based solely on structural neuroimaging. This necessitated microsurgical removal of the neoplasm and blood clot, and, overall, resulted in significant neurological disability. No other cases of major postoperative complications occurred.

3.2. Intraoperative histopathological diagnosis

In 62 cases (90%) the type of the pathological process, namely tumor (with or without more detailed typing and/or grading), cerebral infarction, acute inflammation, and multiple sclerosis, was determined on the intraoperative frozen tissue sections. This rate did not differ significantly between cases with and without the use of ^{1}H-MRS for target selection (28 out of 30 cases [93%] vs. 34 out of 39 cases [87%]; $P = 0.6905$).

In 7 cases (10%) only non-specific histopathological findings were disclosed during intraoperative investigation. In 5 of these cases ^{1}H-MRS-detected metabolic information was not used for target selection. In 3 cases with non-specific findings on the frozen sections, including both after ^{1}H-MRS-supported stereotactic biopsy, further examination of the permanent tissue sections permitted establishment of incomplete diagnosis of low-grade glioma, whereas 4 others remained non-diagnostic. Nevertheless, the association between the use of metabolic data for target selection and establishment of the histopathological diagnosis on permanent tissue sections in cases with unclear intraoperative diagnosis on frozen sections did not reach the level of statistical significance ($P = 0.1429$).

Table 2
Final histopathological diagnosis established on tissue samples obtained with stereotactic brain biopsy in the present series.

Histopathological diagnosis	Number of cases		
	All cases	MRI-guided technique	^{1}H-MRS-supported procedures
Definitive diagnosis			
WHO grade II tumors	28 (40.6%)	14 (35.9%)	14 (46.7%)
Pleomorphic xanthoastrocytoma	1	1	–
Fibrillary astrocytoma	8	5	3
Fibrillary astrocytoma with pilocytic component	1	1	–
Fibrillary astrocytoma with gemistocytic component	1	–	1
Gemistocytic astrocytoma	1	1	–
Diffuse astrocytoma with oligodendroglial component	1	–	1
Diffuse astrocytoma (not other specified)	4	1	3
Oligodendroglioma	5	3	2
Oligodendroglioma with astrocytic component	1	–	1
Oligoastrocytoma	5	2	3
WHO grade III tumors	6 (8.7%)	2 (5.1%)	4 (13.3%)
Anaplastic astrocytoma	3	1	2
Anaplastic astrocytoma with oligodendroglial component	1	–	1
Anaplastic oligodendroglioma	1	–	1
Anaplastic oligoastrocytoma	1	1	–
WHO grade IV tumors	18 (26.1%)	11 (28.2%)	7 (23.3%)
Glioblastoma	7	3	4
Malignant lymphoma	7	5	2
Germinoma	2	1	1
Metastatic carcinoma	2	2	–
Non-neoplastic pathology	5 (7.2%)	3 (7.7%)	2 (6.7%)
Encephalitis	2	1	1
Old cerebral infarction	1	1	–
Multiple sclerosis	2	1	1
Incomplete diagnosis			
Low-grade glioma	8 (11.6%)	5 (12.8%)	3 (10.0%)
Non-diagnostic cases	4 (5.8%)	4 (10.3%)	–
Satellitosis and peritumoral brain	1	1	–
Normal brain tissue with fibrous meningothelial part	1	1	–
Gliofibrillary tissue with necrosis and lymphoid cell infiltration	1	1	–
Chronic inflammation with demyelination	1	1	–
Total number of cases	69 (100%)	39 (100%)	30 (100%)

WHO: World Health Organization.

3.3. *Final histopathological diagnosis and diagnostic yield*

In 57 cases (83%), a definitive histopathological diagnosis was established on the permanent tissue sections. This rate did not differ significantly between cases with and without the use of ^{1}H-MRS for target selection (27 out of 30 cases [90%] vs. 30 out of 39 cases [77%]; $P = 0.2073$).

In 8 patients (11%), incomplete diagnosis of low-grade glioma without precise tumor typing and/or grading was performed. In 4 other patients (6%) the histopathological findings on the permanent tissue sections were non-specific and did not permit establishment of a diagnosis of the lesion (Table 3). In 5 out of 8 cases with incomplete final histopathological diagnosis, and in all non-diagnostic cases, ^{1}H-MRS-detected metabolic data were not used for target selection.

Overall the diagnostic yield of stereotactic biopsy in the present series was 94% (65 out of 69 cases). It was 100% (30 out of 30 cases) in ^{1}H-MRS-supported procedures, compared to 90% (35 out of 39 cases) in MRI-guided tissue sampling ($P = 0.1268$).

3.4. *Diagnostic accuracy*

Comparison of the histopathological diagnoses after stereotactic biopsy and surgical resection in 37 patients who underwent lesion

Table 3
Non-diagnostic cases of stereotactic brain biopsy in the present series.

Case no.	Age, sex	Number of biopsy samples	Diagnosis after stereotactic biopsy	Diagnosis after surgical resection	Contrast enhancement	^{1}H-MRS support
1	65, M	2	Satellitosis and peritumoral brain	Anaplastic oligodendroglioma WHO grade III	No	No
2	16, M	2	Normal brain tissue with fibrous meningothelial part	Focal cortical dysplasia	No	No
3	42, M	4	Gliofibrillary tissue with necroses and lymphoid cell infiltration	Old cerebral infarction	Patchy	No
4	51, M	4	Chronic inflammation and demyelination	Surgery was not done	Patchy	No

M, male; F, female.

removal within a month after initial tissue sampling revealed complete diagnostic agreement in 13 cases (35%). Minor disagreement was noted in 14 cases (38%) and at least one of the following diagnostic errors after stereotactic biopsy was included: designation of WHO grade I tumors as grade II; incomplete histopathological diagnosis or erroneous typing of gliomas with their exact grading; missed diagnosis of the focal cortical dysplasia and old cerebral infarction. Major diagnostic disagreement was noted in 10 cases (27%). Among these 10 cases, initial undergrading of non-enhancing WHO grade III gliomas was the most common (Table 4).

Overall the diagnostic accuracy of stereotactic biopsy in the present series was 73% (27 out of 37 cases). It was 67% (12 out of 18 cases) in ^{1}H-MRS-supported procedures, compared to 79% (15 out of 19 cases) in MRI-guided tissue sampling ($P = 0.4756$).

In 27 cases (73%), the MIB-1 index established at the time of stereotactic biopsy was within the 95% confidence interval of those that was determined after resection of the lesion. This rate did not differ significantly between cases with and without the use of ^{1}H-MRS for target selection (14 out of 18 cases [78%] vs. 13 out of 19 cases [68%]; $P = 0.7140$).

4. Discussion

Targeting in cases of image-guided stereotactic brain biopsy is usually directed on the contrast-enhanced part of the lesion, or on its center, if contrast enhancement is absent [3,50,51]. Possible heterogeneity of the neoplasm, however, creates intrinsic diagnostic limitations for the procedure. Particularly, undergrading of gliomas is not uncommon [1,2,7,16–18]. In the series of Jackson et al. [7], 63% of tumors initially classified as of low or intermediate grade and 60% of anaplastic astrocytomas were found to be more malignant after subsequent surgical resection. Proposed multiple tissue sampling from different parts of the lesion can improve the diagnostic accuracy of stereotactic biopsy [17,50,51]. However, it may be associated with increased risk of major regional complications and neurological deterioration, especially if performed in the eloquent brain areas [22,31].

Additional use of metabolic data for target selection can potentially increase the diagnostic efficacy of stereotactic brain biopsy. Previous reports noted significant improvement of its diagnostic yield if guidance with ^{18}F-fluorodeoxyglucose, L-methyl-^{11}C-methionine, O-2-^{18}F-fluoroethyl-L-tyrosine, ^{18}F-choline and ^{11}C-choline PET [19,22,24,27–33], or ^{201}thallium SPECT [34] was used. These techniques, however, have recognizable disadvantages, such as radiation exposure, excessive time requirements, poor anatomical resolution, technological complexity, and financial expense, which limit their possible use to highly specialized centers [22,24,34,44].

Alternatively, ^{1}H-MRS is a completely non-invasive, extremely sensitive, and highly informative investigation, which can be easily attained at the time of routine MRI. The content of ^{1}H-MRS-detected metabolites reflects certain pathophysiological processes in the investigated volume of tissue [42,43,52–59]. Acquisition of spectroscopic images before planned stereotactic brain biopsy does not require any special equipment and is not accompanied by a significant increase in examination time. Spectroscopic data can be easily incorporated into a computer-based program for neuronavigation. Technical simplicity facilitates routine use of ^{1}H-MRS-support during image-guided stereotactic procedures and there are multiple reports on its effective use for metabolically guided lesion resection [60,61] or biopsy [20,35–42,44,62].

In the present series, the diagnostic yield of ^{1}H-MRS-supported stereotactic tissue sampling was 100%, which is in concordance with

Table 4
Cases with major disagreement of the histopathological diagnoses established after stereotactic biopsy and subsequent surgical resection of the lesion.

Case no.	Age, sex	Number of biopsy samples	Diagnosis after stereotactic biopsy	Diagnosis after surgical resection	Contrast enhancement	^{1}H-MRS support[a]
1	33, M	1	Oligodendroglioma WHO grade II	Anaplastic oligodendroglioma WHO grade III	No	No
2	26, M	1	Fibrillary astrocytoma WHO grade II	Anaplastic astrocytoma with gemistocytic component WHO grade III	Heterogeneous	No
3	54, F	1	Diffuse astrocytoma (not other specified) WHO grade II	Anaplastic oligodendroglioma with astrocytic component WHO grade III	No	No
4	30, M	1	Diffuse astrocytoma (not other specified) WHO grade II	Anaplastic astrocytoma with gemistocytic component WHO grade III	No	Yes (0.56)
5	27, M	1	Diffuse astrocytoma (not other specified) WHO grade II	Anaplastic oligodendroglioma WHO grade III	No	Yes (0.21)
6	58, M	1	Fibrillary astrocytoma with gemistocytic component WHO grade II	Anaplastic astrocytoma WHO grade III	No	Yes (0.30)
7	37, F	2	Oligoastrocytoma WHO grade II	Anaplastic astrocytoma with oligodendroglial component WHO grade III	No	Yes (0.40)
8	32, M	4	Oligoastrocytoma WHO grade II	Anaplastic oligoastrocytoma WHO grade III	No	Yes (0.04)
9	38, M	5	Anaplastic astrocytoma WHO grade III	Oligodendroglioma with astrocytic component WHO grade II	No	Yes (0.72)
10	65, M	2	Satellitosis and peritumoral brain	Anaplastic oligodendroglioma WHO grade III	No	No

M, male; F, female.
Note that Case 10 corresponds to Case 1 in Table 3.
[a] Exact values of NAA/Cho ratio in the target are presented in parentheses.

previous reports on ^{1}H-MRS-guided [35–37,41,44], PET-guided [19,22,29–31], and perfusion-weighted MRI-guided [23] biopsies. However, the difference compared to procedures based solely on structural neuroimaging did not reach the level of statistical significance, probably due to the high diagnostic efficacy of the MRI-guided biopsy itself and the relatively small number of cases in the present series. Moreover, ^{1}H-MRS support was not associated with improved diagnostic accuracy when lesions surgically resected after initial tissue sampling were analyzed separately. This could be caused by incomplete coverage of the tumor with two-dimensional ^{1}H-MRS voxel, a relatively large size of subvoxels, or suboptimal selection of the metabolic target.

Typical ^{1}H-MRS-detected metabolic abnormalities in brain tumors include increase of Cho, decreases of NAA and Cr, and frequent appearance of Lac and Lip [14,21,43,52,56,58,62]. Cho is associated with both synthesis and degradation of cell membranes, and its increase may reflect high cellularity, active proliferation, inflammation, or early necrotic processes. NAA is nearly selectively distributed in neurons, and reflects their density, viability, and functional activity. It was shown previously that increase of proliferative activity and malignant progression of parenchymal brain tumors are generally correlated with increase of Cho and Lip contents and decrease of NAA content, while some highly malignant neoplasms with extensive necroses may have lower Cho content compared to their more benign counterparts [42,43,52–59]. In a clinical setting, the content of metabolites is usually expressed semiquantitatively as various metabolic ratios. The NAA/Cho ratio, which was used in the present series for the selection of the target for stereotactic biopsy, is a validated marker of the tumor presence, proliferative activity, and growth characteristics [20,24,38–40,42,52,53,57,63]. In our own retrospective analysis of various ^{1}H-MRS-detected metabolic parameters in differentiation of 71 high-grade and low-grade gliomas, the NAA/Cho ratio showed the strongest discriminative power [64]. Nevertheless, it may be not specific enough for precise determination of the histopathological tumor grade in each individual case [24,52,57,63]. Recently, Ng and Lim [45] showed that direction of the tissue sampling on the area with the lowest NAA/Cho might lead to erroneous diagnosis of anaplastic astrocytoma in cases of glioblastomas. In concordance with their report, the results presented herein permit us to conclude that tissue sampling from the area of the lowest NAA/Cho ratio may result in undergrading of the non-enhancing WHO grade III gliomas. This was observed in 5 out of 6 cases with major diagnostic errors after ^{1}H-MRS-supported stereotactic brain biopsy in the present series (Table 4).

Other metabolic targets for ^{1}H-MRS-guided tissue sampling have been used previously. McKnight et al. [42] recommended selection of the biopsy target based both on the maximal value of Cho/NAA ratio and the originally developed Cho-to-NAA index, which reflects the number of standard deviations of difference between the relative level of Cho in a given voxel and the mean relative level of Cho in voxels from non-tumor regions. In a limited number of patients Son et al. [37] obtained tissue samples from the areas of increased Cho/Cr, decreased NAA/Cr and elevated Lac signal, and found good histopathological correspondence in all cases. In 26 patients with parenchymal brain tumors, including 16 after previous irradiation, Martin et al. [36] directed the biopsy on the area of highest Cho signal intensity compared to its level in the normal brain. It was effective in 17 out of 21 histologically confirmed tumors, but four malignant neoplasms did not exhibit elevation of Cho, which precluded their definitive metabolic targeting. Hermann et al. [44] used a similar technique with a 3 T MR scanner and attained 89% diagnostic accuracy in discrimination between non-enhancing WHO grade II and grade III gliomas. In 2 cases of malignant gliomas, Ng and Lim [45] advocated tissue sampling from the area with the highest Lip content. Nevertheless, direct comparison of the histopathological diagnoses obtained with ^{1}H-MRS-supported stereotactic biopsy and subsequent surgical resection of the lesion was not performed in any previous study.

While advantages of ^{1}H-MRS-supported tissue sampling over MRI-guided technique were not statistically proved in the present study, some indications for metabolic guidance during stereotactic brain biopsies may be considered reasonable. First, it may be extremely helpful in lesions progressing after irradiation, with frequent co-existence of radiation-induced necrosis and viable neoplasm [36,38,39,41,43,62,63,65]. Second, detection of the metabolic abnormalities outside the contrast-enhanced area of the highly vascular tumor can make it possible to obtain a representative tissue specimen with reduced risk of hemorrhagic complications [51,63]. Further testing of other ^{1}H-MRS-detected parameters, particularly the evaluation of the relative content of Lip and pattern analysis of the pathological spectrum [45,64], may facilitate optimal selection of the metabolic target for tissue sampling. Finally, introduction of MR scanners with high magnetic field strength (3 T and more) for spectroscopic imaging can provide an opportunity to use smaller voxel size with good signal-to-noise ratio, acceptable acquisition time, and better spectral resolution, which may result in more precise navigation of stereotactic brain biopsy [44].

5. Conclusion

In the present series, the use of ^{1}H-MRS-support for frame-based image-guided stereotactic biopsy of parenchymal brain lesions resulted in 100% diagnostic yield and 67% diagnostic accuracy. These parameters, however, did not differ significantly from an MRI-based technique. Further search for optimal metabolic targets is necessary for the improvement of the diagnostic efficacy of spectroscopic navigation during tissue sampling, particularly in cases of non-enhancing intermediate grade gliomas.

Acknowledgements

This work was supported by the Program for Promoting the Establishment of Strategic Research Centers, Special Coordination Funds for Promoting Science and Technology, Ministry of Education, Culture, Sports, Science and Technology (Japan). The authors are thankful to Dr. Craig Gough for helping with manuscript preparation.

References

[1] Blaauw G, Braakman R. Pitfalls in diagnostic stereotactic brain surgery. Acta Neurochir Suppl 1988;42:161–5.
[2] Voges J, Schroder R, Treuer H, Pastyr O, Schlegel W, Lorenz WJ, et al. CT-guided and computer assisted stereotactic biopsy: technique, results, indications. Acta Neurochir (Wien) 1993;125:142–9.
[3] Soo TM, Bernstein M, Provias J, Tasker R, Lozano A, Guha A. Failed stereotactic biopsy in a series of 518 cases. Stereotact Funct Neurosurg 1996;64:183–96.
[4] Hall WA. The safety and efficacy of stereotactic biopsy for intracranial lesions. Cancer 1998;82:1749–55.
[5] Fontaine D, Dormont D, Hasboun D, Clemenceau S, Valery C, Oppenheim C, et al. Magnetic resonance-guided stereotactic biopsies: results in 100 consecutive cases. Acta Neurochir (Wien) 2000;142:249–56.
[6] Yu X, Liu Z, Tian Z, Li S, Huang H, Xiu B, et al. Stereotactic biopsy for intracranial space-occupying lesions: clinical analysis of 550 cases. Stereotact Funct Neurosurg 2000;75:103–8.
[7] Jackson RJ, Fuller GN, Abi-Said D, Lang FF, Gokaslan ZL, Shi WM, et al. Limitations of stereotactic biopsy in the initial management of gliomas. Neurooncology 2001;3:193–200.
[8] Kim JE, Kim DG, Paek SH, Jung HW. Stereotactic biopsy for intracranial lesions: reliability and its impact on the planning of treatment. Acta Neurochir (Wien) 2003;145:547–55.
[9] Takahashi H, Sugai T, Uzuka T, Kano M, Honma J, Grinev I, et al. Complications and diagnostic yield of stereotactic biopsy for the patients with malignant brain tumors. No Shinkei Geka 2004;32:135–40 (in Japanese).

[10] Yamada K, Goto S, Kochi M, Ushio Y. Stereotactic biopsy for multifocal, diffuse, and deep-seated brain tumors using Leksell's system. J Clin Neurosci 2004;11:263–7.
[11] Aker FV, Hakan T, Karadereler S, Erkan M. Accuracy and diagnostic yield of stereotactic biopsy in the diagnosis of brain masses: comparison of results of biopsy and resected surgical specimens. Neuropathology 2005;25:207–13.
[12] Heper AO, Erden E, Savas A, Ceyhan K, Erden I, Akyar S, et al. An analysis of stereotactic biopsy of brain tumors and nonneoplastic lesions: a prospective clinicopathologic study. Surg Neurol 2005;64(Suppl. 2):S82–8.
[13] Jain D, Sharma MC, Sarkar C, Deb P, Gupta D, Mahapatra AK. Correlation of diagnostic yield of stereotactic brain biopsy with number of biopsy bits and site of the lesion. Brain Tumor Pathol 2006;23:71–5.
[14] Setzer M, Herminghaus S, Marquardt G, Tews DS, Pilatus U, Seifert V, et al. Diagnostic impact of proton MR-spectroscopy versus image-guided stereotactic biopsy. Acta Neurochir (Wien) 2007;149:379–86.
[15] Kleihues P, Volk B, Anagnostopoulos J, Kiessling M. Morphologic evaluation of stereotactic brain tumour biopsies. Acta Neurochir Suppl 1984;33:171–81.
[16] Chandrasoma PT, Smith MM, Apuzzo MLJ. Stereotactic biopsy in the diagnosis of brain masses: comparison of results of biopsy and resected surgical specimen. Neurosurgery 1989;24:160–5.
[17] Feiden W, Steude U, Bise K, Gundisch O. Accuracy of stereotactic brain tumor biopsy: comparison of the histologic findings in biopsy cylinders and resected tumor tissue. Neurosurg Rev 1991;14:51–6.
[18] McGirt MJ, Villavicencio AT, Bulsara KR, Friedman AH. MRI-guided stereotactic biopsy in the diagnosis of glioma: comparison of biopsy and surgical resection specimen. Surg Neurol 2003;59:277–82.
[19] Levivier M, Goldman S, Pirotte B, Brucher JM, Baleriaux D, Luxen A, et al. Diagnostic yield of stereotactic brain biopsy guided by positron emission tomography with [^{18}F]fluorodeoxyglucose. J Neurosurg 1995;82:445–52.
[20] Croteau D, Scarpace L, Hearshen D, Gutierrez J, Fisher JL, Rock JP, et al. Correlation between magnetic resonance spectroscopy imaging and image-guided biopsies: semiquantitative and qualitative histopathological analyses of patients with untreated glioma. Neurosurgery 2001;49:823–9.
[21] Law M, Yang S, Wang H, Babb JS, Johnson G, Cha S, et al. Glioma grading: sensitivity, specificity, and predictive values of perfusion MR imaging and proton MR spectroscopic imaging compared with conventional MR imaging. AJNR Am J Neuroradiol 2003;24:1989–98.
[22] Pirotte B, Goldman S, Salzberg S, Wikler D, David P, Vandesteene A, et al. Combined positron emission tomography and magnetic resonance imaging for the planning of stereotactic brain biopsies in children: experience in 9 cases. Pediatr Neurosurg 2003;38:146–55.
[23] Maia Jr ACM, Malheiros SMF, da Rocha AJ, Stavale JN, Guimaraes IF, Borges LRR, et al. Stereotactic biopsy guidance in adults with supratentorial nonenhancing gliomas: role of perfusion-weighted magnetic resonance imaging. J Neurosurg 2004;101:970–6.
[24] Floeth FW, Pauleit D, Wittsack H-J, Langen KJ, Reifenberger G, Hamacher K, et al. Multimodal metabolic imaging of cerebral gliomas: positron emission tomography with [^{18}F]fluoroethyl-L-tyrosine and magnetic resonance spectroscopy. J Neurosurg 2005;102:318–27.
[25] Maia ACM, Malheiros SMF, da Rocha AJ, da Silva CJ, Gabbai AA, Ferraz FAP, et al. MR cerebral blood volume maps correlated with vascular endothelial growth factor expression and tumor grade in nonenhancing gliomas. AJNR Am J Neuroradiol 2005;26:777–83.
[26] Rollin N, Guyotat J, Streichenberger N, Honnorat J, Tran Minh V-A, Cotton F. Clinical relevance of diffusion and perfusion magnetic resonance imaging in assessing intra-axial brain tumors. Neuroradiology 2006;48:150–9.
[27] Hanson MW, Glantz MJ, Hoffman JM, Friedman AH, Burger PC, Schold SC, et al. FDG-PET in the selection of brain lesions for biopsy. J Comput Assist Tomogr 1991;15:796–801.
[28] Levivier M, Goldman S, Bidaut L, Luxen A, Stanus E, Przedborski S, et al. Proton emission tomography-guided stereotactic brain biopsy. Neurosurgery 1992;31:792–7.
[29] Maciunas RJ, Kessler RM, Maurer C, Mandava V, Watt G, Smith G. Positron emission tomography imaging-directed stereotactic neurosurgery. Stereotact Funct Neurosurg 1992;58:134–40.
[30] Pirotte B, Goldman S, David P, Wikler D, Damhaut P, Vandesteene A, et al. Stereotactic brain biopsy guided by positron emission tomography (PET) with [F-18]fluorodeoxyglucose and [C-11]methionine. Acta Neurochir Suppl 1997;68:133–8.
[31] Massager N, David P, Goldman S, Pirotte B, Wikler D, Salmon I, et al. Combined magnetic resonance imaging- and positron emission tomography-guided stereotactic biopsy in brainstem mass lesions: diagnostic yield in a series of 30 patients. J Neurosurg 2000;93:951–7.
[32] Messing-Junger AM, Floeth FW, Pauleit D, Reifenberger G, Willing R, Gartner J, et al. Multimodal target point assessment for stereotactic biopsy in children with diffuse bithalamic astrocytomas. Childs Nerv Syst 2002;18:445–9.
[33] Hara T, Kondo T, Hara T, Kosaka N. Use of ^{18}F-choline and ^{11}C-choline as contrast agents in positron emission tomography imaging-guided stereotactic biopsy sampling of gliomas. J Neurosurg 2003;99:474–9.
[34] Hemm S, Vayssiere N, Zanca M, Ravel P, Coubes P. Thallium SPECT-based stereotactic targeting for brain tumor biopsies. Stereotact Funct Neurosurg 2004;82:70–6.
[35] Hall WA, Martin A, Liu H, Truwit CL. Improving diagnostic yield in brain biopsy: coupling spectroscopic targeting with real-time needle placement. J Magn Reson Imaging 2001;13:12–5.
[36] Martin AJ, Liu H, Hall WA, Truwit CL. Preliminary assessment of turbo spectroscopic imaging for targeting in brain biopsy. AJNR Am J Neuroradiol 2001;22:959–68.
[37] Son BC, Kim MC, Choi BG, Kim EN, Baik HM, Choe BY, et al. Proton magnetic resonance chemical shift imaging (^{1}H CSI)-directed stereotactic biopsy. Acta Neurochir (Wien) 2001;143:45–50.
[38] Rock JP, Hearshen D, Scarpace L, Croteau D, Gutierrez J, Fisher JL, et al. Correlations between magnetic resonance spectroscopy and image-guided histopathology, with special attention to radiation necrosis. Neurosurgery 2002;51:912–20.
[39] Rock JP, Scarpace L, Hearshen D, Gutierrez J, Fisher JL, Rosenblum M, et al. Associations among magnetic resonance spectroscopy, apparent diffusion coefficients, and image-guided histopathology with special attention to radiation necrosis. Neurosurgery 2004;54:1111–9.
[40] Ganslandt O, Stadlbauer A, Fahlbusch R, Kamada K, Buslei R, Blumcke I, et al. Proton magnetic resonance spectroscopic imaging integrated into image-guided surgery: correlation to standard magnetic resonance imaging and tumor cell density. Neurosurgery 2005;56(Suppl. 2)):291–8.
[41] Hall WA, Truwit CL. 1.5 T: spectroscopy-supported brain biopsy. Neurosurg Clin N Am 2005;16:165–72.
[42] McKnight TR, Lamborn KR, Love TD, Berger MS, Chang S, Dillon WP, et al. Correlation of magnetic resonance spectroscopic and growth characteristics within Grades II and Grades III gliomas. J Neurosurg 2007;106:660–6.
[43] Sibtain NA, Howe FA, Saunders DE. The clinical value of proton magnetic resonance spectroscopy in adult brain tumours. Clin Radiol 2007;62:109–19.
[44] Hermann EJ, Hattingen E, Krauss JK, Marquardt G, Pilatus U, Franz K, et al. Stereotactic biopsy in gliomas guided by 3-Tesla ^{1}H-chemical-shift imaging of choline. Stereotact Funct Neurosurg 2008;86:300–7.
[45] Ng WH, Lim T. Targeting regions with highest lipid content on MR spectroscopy may improve diagnostic yield in stereotactic biopsy. J Clin Neurosci 2008;15:502–6.
[46] Muragaki Y, Chernov M, Maruyama T, Ochiai T, Taira T, Kubo O, et al. Low-grade glioma on stereotactic biopsy: how often is the diagnosis accurate? Minim Invasive Neurosurg 2008;51:275–9.
[47] Louis DN, Ohgaki H, Wiestler OD, Cavenee WK, editors. WHO Classification of Tumours of the Central Nervous System. Lyon: IARC; 2007.
[48] Mork SJ, Halvorsen TB, Lindegaard K-F, Eide GE. Oligodendroglioma: histologic evaluation and prognosis. J Neuropathol Exp Neurol 1986;45:65–78.
[49] Muragaki Y, Iseki H, Maruyama T, Kawamata T, Yamane F, Nakamura R, et al. Usefulness of intraoperative magnetic resonance imaging for glioma surgery. Acta Neurochir Suppl 2006;98:67–75.
[50] Kelly PJ, Daumas-Duport C, Kispert DB, Kall BA, Scheithauer BW, Illig J. Imaging-based stereotaxic serial biopsies in untreated intracranial glial neoplasms. J Neurosurg 1987;66:865–74.
[51] Greene GM, Hitchon PW, Schelper RL, Yuh W, Dyste GN. Diagnostic yield in CT-guided stereotactic biopsy of gliomas. J Neurosurg 1989;71:494–7.
[52] Negendank WG, Sauter R, Brown TR, Evelhoch JL, Falini A, Gotsis ED, et al. Proton magnetic resonance spectroscopy in patients with glial tumors: a multicenter study. J Neurosurg 1996;84:449–58.
[53] Shimizu H, Kumabe T, Tominaga T, Kayama T, Hara K, Ono Y, et al. Noninvasive evaluation of malignancy of brain tumors with proton MR spectroscopy. AJNR Am J Neuroradiol 1996;17:737–47.
[54] Tedeschi G, Lundbom N, Raman R, Bonavita S, Duyn JH, Alger JR, et al. Increased choline signal coinciding with malignant degeneration of cerebral gliomas: a serial proton magnetic resonance spectroscopy imaging study. J Neurosurg 1997;87:516–24.
[55] Meyerand ME, Pipas JM, Mamourian A, Tosteson TD, Dunn JF. Classification of biopsy-confirmed brain tumors using single-voxel MR spectroscopy. AJNR Am J Neuroradiol 1999;20:117–23.
[56] Shimizu H, Kumabe T, Shirane R, Yoshimoto T. Correlation between choline level measured by proton MR spectroscopy and Ki-67 labeling index in gliomas. AJNR Am J Neuroradiol 2000;21:659–65.
[57] Tamiya T, Kinoshita K, Ono Y, Matsumoto K, Furuta T, Ohmoto T. Proton magnetic resonance spectroscopy reflects cellular proliferative activity in astrocytomas. Neuroradiology 2000;42:333–8.
[58] Moller-Hartmann W, Herminghaus S, Krings T, Marquardt G, Lanfermann H, Pilatus U, et al. Clinical application of proton magnetic resonance spectroscopy in the diagnosis of intracranial mass lesions. Neuroradiology 2002;44:371–81.
[59] Calvar JA, Meli FJ, Romero C, Calcagno ML, Yanez P, Martinez AR, et al. Characterization of brain tumors by MRS, DWI and Ki-67 labeling index. J Neurooncol 2005;72:273–80.
[60] Preul MC, Leblanc R, Caramanos Z, Kasrai R, Narayanan S, Arnold DL. Magnetic resonance spectroscopy guided brain tumor resection: differentiation between recurrent glioma and radiation change in two diagnostically difficult cases. Can J Neurol Sci 1998;25:13–22.
[61] Stadlbauer A, Moser E, Gruber S, Nimsky C, Fahlbusch R, Ganslandt O. Integration of biochemical images of a tumor into frameless stereotaxy achieved using a magnetic resonance imaging/magnetic resonance spectroscopy hybrid data set. J Neurosurg 2004;101:287–94.
[62] Dowling C, Bollen AW, Noworolski SM, McDermott MW, Barbaro NM, Day MR, et al. Preoperative proton MR spectroscopic imaging of brain tumors: correlation with histopathologic analysis of resection specimens. AJNR Am J Neuroradiol 2001;22:604–12.

[63] Burtscher IM, Skagerberg G, Geijer B, Englund E, Stahlberg F, Holtas S. Proton MR spectroscopy and preoperative diagnostic accuracy: an evaluation of intracranial mass lesions characterized by stereotactic biopsy findings. AJNR Am J Neuroradiol 2000;21:84–93.
[64] Chernov MF, Ono Y, Muragaki Y, Kubo O, Nakamura R, Iseki H, et al. Differentiation of high-grade and low-grade gliomas using pattern analysis of long-echo single-voxel proton magnetic resonance spectroscopy (^{1}H-MRS). Neuroradiol J 2008;21:338–49.
[65] Chernov MF, Hayashi M, Izawa M, Usukura M, Yoshida S, Ono Y, et al. Multivoxel proton MRS for differentiation of radiation-induced necrosis and tumor recurrence after gamma knife radiosurgery for brain metastases. Brain Tumor Pathol 2006;23:19–27.